View metadata, citation and similar papers at core.ac.uk

brought to you by CORE

provided by Warwick Research Archives Portal Repository

Manuscript version: Author's Accepted Manuscript
The version presented in WRAP is the author's accepted manuscript and may differ from the published version or Version of Record.

Persistent WRAP URL:
http://wrap.warwick.ac.uk/101928

How to cite:
Please refer to published version for the most recent bibliographic citation information. If a published version is known of, the repository item page linked to above, will contain details on accessing it.

Copyright and reuse:
The Warwick Research Archive Portal (WRAP) makes this work by researchers of the University of Warwick available open access under the following conditions.

Copyright © and all moral rights to the version of the paper presented here belong to the individual author(s) and/or other copyright owners. To the extent reasonable and practicable the material made available in WRAP has been checked for eligibility before being made available.

Copies of full items can be used for personal research or study, educational, or not-for-profit purposes without prior permission or charge. Provided that the authors, title and full bibliographic details are credited, a hyperlink and/or URL is given for the original metadata page and the content is not changed in any way.

Publisher's statement:
Please refer to the repository item page, publisher's statement section, for further information.

For more information, please contact the WRAP Team at: wrap@warwick.ac.uk.

warwick.ac.uk/lib-publications

The potential of zwitterionic nanoliposomes against neurotoxic alpha-synuclein aggregates in Parkinson's Disease

Farhang Aliakbari [1,2,3], Hossein Mohammad-Beigi [1,2,4], Nasrollah Rezaei-Ghaleh [5], Stefan Becker [6], Faezeh Dehghani Esmatabad [1], Hadieh Alsadat Eslampanah Seyedi [1,7], Hassan Bardania [8], Amir Tayaranian Marvian [1,9], Joanna F. Collingwood [10], Gunna Christiansen [11], Markus Zweckstetter [5,6,12], Daniel E. Otzen[* 2] and Dina Morshedi[*1]

1. Bioprocess Engineering Department, Institute of Industrial and Environmental Biotechnology, National Institute of Genetic Engineering and Biotechnology, Tehran, Iran.
2. Interdisciplinary Nanoscience Centre (iNANO) and Department of Molecular Biology and Genetics, Aarhus University, Gustav Wieds Vej 14, DK–8000 Aarhus C, Denmark.
3. Department & Center for Biotechnology Research, School of Medicine, Semnan University of Medical Sciences, Semnan, Iran.
4. Biotechnology Group, Faculty of Chemical Engineering, Tarbiat Modares University, P.O. Box 14115-143, Tehran, Iran.
5. Department of Neurology, University Medical Center Göttingen, Germany.
6. Department for NMR-based Structural Biology, Max Planck Institute for Biophysical Chemistry, Göttingen, Germany.
7. Institute for Glycomics, Griffith University, QLD, Australia.
8. Cellular and Molecular Research Center, Yasuj University of Medical Sciences, Yasuj, Iran.
9. Department of Translational Neurodegeneration, German Center for Neurodegenerative Diseases (DZNE), D-81377, Munich, Germany.
10. School of Engineering, University of Warwick, Coventry, UK.
11. Department of Biomedicine, Aarhus University, 8000 Aarhus C, Denmark.
12. German Center for Neurodegenerative Diseases (DZNE), Göttingen, Germany.

*** Corresponding Authors**:

morshedi@nigeb.ac.ir (Morshedi. D.), National Institute of Genetic Engineering and Biotechnology, Address: Shahrak-e Pajoohesh, km 15 Tehran - Karaj Highway, Tehran, Iran, P.O.Box:14965/161,Tehran,Iran, Tel: +9821-44878423, Fax: +9821-44878395

dao@inano.au.dk (Otzen. D. E.), Interdisciplinary Nanoscience Centre (iNANO) and Department of Molecular Biology and Genetics, Aarhus University, Gustav Wieds Vej 14, building 1592, 224.8000 Aarhus C, Denmark. Mobile: +4520725238

Abstract

The protein α-synuclein (αSN) aggregates to form fibrils in neuronal cells of Parkinson's patients. Here we report on the effect of neutral (zwitterionic) nanoliposomes (NLPs), supplemented with cholesterol (NLP-Chol) and decorated with PEG (NLP-Chol-PEG), on αSN aggregation and neurotoxicity. Both NLPs retard αSN fibrillization in a concentration-independent fashion. They do so largely by increasing lag time (formation of fibrillization nuclei) rather than elongation (extension of existing nuclei). Interactions between neutral NLPs and αSN may locate to the N-terminus of the protein. This interaction can even perturb the interaction of αSN with negatively charged NLPs which induces an α-helical structure in αSN. This interaction was found to occur throughout the fibrillization process. Both NLP-Chol and NLP-Chol-PEG were shown to be biocompatible *in vitro,* and to reduce αSN neurotoxicity and reactive oxygen species (ROS) levels with no influence on intracellular calcium in neuronal cells, emphasizing a prospective role for NLPs in reducing αSN pathogenicity *in vivo* as well as utility as a vehicle for drug delivery.

Keywords: α-Synuclein, Fibrillization, Neurotoxicity, Parkinson’s disease, Zwitterionic nanoliposomes.

Author contribution:

D.M, D.E.O and F.A devised the project, the main conceptual ideas and proof outline. F.A worked out almost all of the experiment design, and performed the numerical calculations for the suggested experiment. H.M-B, H.B as well as F.D.E, H.A.E.S, and A.T.M helped to carry out the experiment and performed the calculations. N.R-G worked out the NMR experiment. S.B prepared isotopically-labeled synuclein for NMR experiments. G.C worked out the TEM experiment. F.A, H.M-B, N.R-G, S.B, H.B, A.T.M, J.F.C, G.C, M.Z, D.E.O and D.M analyzed the data. F.A wrote the manuscript with support from J.F.C, M.Z and more importantly and largely D.E.O as well as D.M. All authors discussed the results and contributed to the final manuscript.

Introduction

Alpha synuclein (αSN) is a 140-residue natively unfolded protein found in high concentrations in neuronal cells. Patients suffering from a range of neurodegenerative disorders show neuronal deposits of plaque-like intracellular structures named Lewy bodies and Lewy neurites with a high content of aggregated αSN [1]. Although the physiological function of αSN remains unresolved, degeneration of neurons in the affected region of the brain is linked to αSN aggregation [2]. Therefore, insight into events triggering fibrillization is crucial for neuroprotective strategies against so-called α-synucleinopathies. While many compounds have been shown to inhibit αSN aggregation *in vitro* [3–5], this still remains to be translated into successful treatment *in vivo* [6,7]. Therapeutic strategies must also address the fact that αSN aggregates can spread to other cells [8,9]. The membranes of all mammalian cells are enriched in phosphatidylcholine lipids while those of neurons are enriched with neutral lipids and cholesterol [10–12]. αSN shows great affinity for membranes, particularly those with anionic lipids, and binding is mediated by the N-terminal amphipathic domain. The extent of membrane-bound αSN may play a key role in αSN biological functions as well as the initiation and kinetics of its aggregation [10,13], all of which is affected by the composition (charge, fluidity) and size (*i.e.* curvature) of liposomal membranes.

Anionic vesicles interact strongly with αSN, inducing an α-helical structure [14], while other vesicles have no such effect [15]. Besides charge, the lipid phase also plays a role: αSN interacts more strongly with the fluid phase than the gel phase and fibril formation has been reported to develop in the presence of lipids in the fluid phase [16]. The local increase in αSN concentration on the membrane may also promote aggregation through nucleus formation, making the protein:lipid ratio a critical parameter [16–21].

Given that αSN membrane interactions are complex and unexpected, these aspects must obviously be taken into account when considering liposomal nanocarriers for delivery of drugs that target αSN [14,16,21,22]. Liposomal nanocarriers have properties that are advantages if they are to be used in the body, such as biocompatibility, straightforward surface modification, low immunogenicity and protection against enzymatic degradation [23,24]. However, their potential has been challenged by concerns about possible neurotoxicity [25–28].

Here we report on the effect of zwitterionic (*i.e.* overall uncharged) modified dipalmitoylphosphatidylcholine (DPPC) NLPs on αSN aggregation *in vitro* and their ability to protect two dopaminergic cell lines, PC12 and SHSY5Y, against αSN aggregates. Our choice of uncharged liposomes for NLPs was motivated by the fact that charged liposomes are generally more toxic [25,27] and can promote αSN aggregation [14], while uncharged liposomes are more compatible with the neuronal plasma membrane [11,29]. NLPs were formulated to contain either cholesterol (NLP-Chol) or cholesterol with PEG (NLP-Chol-PEG). Cholesterol regulates the structure, activity and fluidity of biomembranes, particularly in neuronal cells[30] while PEG increases the stability of nanoparticles against enzymatic degradation during blood circulation as well as increasing solubility. Calorimetric studies confirmed that the NLPs were in the gel phase under all experimental conditions. In this work we investigated the effect of NLPs on αSN aggregation kinetics, antioxidant activity, neuronal cytotoxicity, biocompatibility and intracellular calcium levels. We conclude that these NLPs constitute a promising nanocarrier in the context of αSN-related neurodegenerative disease.

MATERIALS AND METHODS

Materials: Thioflavin T (ThT), 3-(4,5-dimethylthiazol-2-yl)-2,5-diphenyltetrazolium bromide (MTT), 2',7'-dichlorodihydrofluorescin diacetate (DCFH-DA) and cholesterol were from Sigma-

Aldrich (St Louis, MO). Lactate dehydrogenase (LDH) measurement kit was from Pishtazteb Co. (Iran). 1,2-Dipalmitoyl-sn-glycero-3-phosphocholine (DPPC), 1,2-dioleoylsn-3-phosphatidylglycerol (DOPG), 1,2-distearoyl-sn-glycero-3-phosphoethanolamine-N-[methoxy (polyethylene glycol)-2000] (PEG2000 PE), and Mini-Extruder were from Avanti Polar Lipids, Inc. (Alabaster, AL, USA). Fura-2AM was from Santa Cruz (American, CA). Annexin-V-FLUOS Staining Kit was from Roche Applied Science (Mannheim, Germany). PC12 and SHSY5Y cell lines were from The Pasteur Institute of Iran. All salts and organic solvents were from Merck (Darmstadt, Germany). Cell culture media (DMEM high glucose and DMEM-F12) and antibiotics were from GibcoBRL (Life Technologies, Paisley, Scotland). Fetal bovine serum (FBS) was from Biosera (Tehran, Iran).

Small Unilamellar Vesicles (SUVs) formulation and characterization

Thin film hydration was employed to make liposomes. DPPC was dissolved in 2 mL chloroform and a thin film of lipid was prepared using rotary evaporator at 37 °C with 150 rpm shaking in a round-bottomed flask. The lipid film was hydrated with phosphate buffer saline (PBS; 8 g/L NaCl, 0.2 g/L KCl, 1.44 g/L Na_2HPO_4 and 0.24 g/L KH_2PO_4, pH 7.4) at 50 °C for 2 hours. Small Unilamellar Vesicles (SUV) with diameter ≤ 100 nm were prepared by extruding the lipid suspension through a 100 nm membrane 21 times using a Mini-Extruder set. To formulate NLPs containing cholesterol and PEG, they were mixed with DPPC at molar ratios of 15% and 10% respectively and dissolved in 2 mL chloroform, followed by the procedures above. NLPs were stored at 4 °C until use. Dynamic light scattering (DLS) using a Zetasizer (Malvern, UK) determined that the SUVs were almost neutral (by ζ potential measurement, between -1.301±0.624 mV to -2.582±0.395 mV) and had a size of ≤ 100 nm. The sizes of NLPs estimated by DLS (z-average) based on number were 85.86±2.04 (PdI 0.2±0.13) and 88.47±1.03 (PdI 0.14±0.017) for NLP-Chol and NLP-Chol-PEG, respectively.

Protein production

Escherichia coli BL21 (DE3) pLysS cells (Novagen, Madison, Wis., U.S.A.) were used to express the wild type recombinant human αSN which was purified as described in Supplementary Information [4].

αSN fibrillization, seeding and the fibril formation assays

αSN was dissolved to 70 μM in PBS supplemented with 200 μM phenylmethylsulfonyl fluoride (PMSF), 1 mM Ethylenediaminetetraacetic acid (EDTA) and 0.05 mM NaN_3 and then centrifuged for 10 minutes at 13000 rpm to remove aggregates. The supernatant of the solution was mixed with 35-1500 μM NLP-Chol and NLP-Chol-PEG (based on DPPC concentration). Fibrillization was carried out by incubation at 37 °C while shaking at 300 rpm in a 96-well plate (see SI for details). The Finke–Watzky two step model [31] was fitted to the normalized ThT fluorescence intensity data:

$$F(t) = \frac{1}{1+e^{-4v(t-t_{1/2})}} \qquad (1)$$

$$t_N = t_{1/2} - \frac{1}{2v} \qquad (2)$$

where $t_{1/2}$ is the time to reach 50% fibrillization, v is the growth rate, and t_N is the length of the nucleation phase. For seeding experiments, fibrils isolated from the plateau phase of fibrillization were collected and sonicated for 5 min in an ultrasonic bath sonicator (Bandelin Sonorex Ultrasonic baths Digital 10P, Germany) at 50% amplitude. Samples without NLPs were included as a control. Additional details are provided in the SI.

NMR spectroscopy

NMR samples contained 0.1 mM ^{15}N-labelled αSN in 17 mM HEPES buffer, 33 mM NaCl, pH 7.4. The internal standard (DSS, 0.4 mM) was used for chemical shift referencing (0 ppm) and intensity calibration. NMR experiments were recorded on a Bruker 600 MHz spectrometer equipped with a cryogenic probe. The 2D ^{15}N–^{1}H HSQC spectra were obtained at 15 °C, using a long recycle delay of 5 s and 512 data points in the ^{15}N dimension. NMR data processing and analysis were performed using NMRPipe and Sparky.

To probe the potential interaction of αSN with liposomes, HSQC spectra were recorded in the absence and the 10-fold excess of cholesterol-containing liposomes either with or without PEG. Intensity perturbation profiles were obtained by comparing intensities of HSQC cross-peaks observed in the presence (I) and absence (I_0) of liposomes.

Oligomer preparation

12 mg/mL αSN was dissolved in PBS and incubated for 2 hours at 37°C with 900 rpm shaking. The sample was centrifuged for 10 min at 13000 rpm to remove insoluble aggregates, incubated for an additional 30 minutes in the same condition, centrifuged again for 10 min at 13000 rpm followed by oligomer purification on a Superose^{TM} 6 10/300 GL, Prep Grade column (GE healthcare Life Sciences, Sweden) at 2.5 mL/min in PBS. Oligomer fractions were concentrated on a 15 mL stirred-cell Amicon unit using a cut-off filter of 30 kDa (Merck).

Calcein release

DOPG vesicles containing calcein at self-quenching concentrations (70 mM) were prepared as described [32]. Briefly, 5 mg/mL DOPG and 70 mM of calcein were dissolved in 1 mL PBS, subjected to 10 times freezing in liquid nitrogen and thawing at 50 °C, extruded 21 times through a 100 nm filter and purified on a PD-10 desalting column (GE Healthcare). The vesicles were

added at final lipid concentration of 42 μM to a 96-well plate in a 150 μL assay solution in PBS together with oligomers and/or NLPs at final concentrations of 0.25 μM and 10-80 μM, respectively. Oligomer-NLPs mixtures were mixed and pre-incubated for 2 min at room temperature and then added to vesicles. Calcein release was followed for 30 min at 37°C on a Genios Pro fluorescence plate reader (Tecan, Mänerdorf, Switzerland) with 485 nm excitation and emission at 520 nm. Afterwards complete lysis was achieved by adding 1 μL Triton X-100 (0.1% (w/v)) and end-level fluorescence intensity measured. Background fluorescence was subtracted. The percentage of calcein release was calculated as follows:

$$\%\ of\ calcein\ release = \frac{(F - F_0)}{(F_t - F_0)} \qquad (3)$$

where F is the fluorescence intensity after adding oligomer-NLPs mixtures, F_0 is the fluorescence intensity before adding the materials and F_t is the fluorescence intensity after treatment with Triton X-100.

Hemolysis assay

100 μL NLPs (lipid concentration 280 μM), were spread onto blood agar medium and incubated for 24 hours at 37 °C. As a control, 100 μL of a suspension of *Bacillus Cereus* (0.5 McFarland) was cultured on the same medium.

Effect of NLPs on αSN neurotoxicity

The neurotoxicity of αSN (with and without NLPs), towards the dopaminergic cell lines PC12, SHSY5Y, and SHSY5Y over-expressing αSN, were evaluated by MTT and LDH assays, flow cytometry (to detect early apoptosis and late apoptosis/necrosis), ROS measurement, and measurement of intracellular calcium. Cells were cultured for 24 hours in DMEM high glucose or DMEM-F12 for PC12 and SHSY5Y, respectively supplemented with 10% FBS, 100 U/mL

penicillin and 100 µg/mL streptomycin and incubated at 37 °C in humidified atmosphere with 5% CO_2 and 90% humidity. The cells were then cultured in 96-well microtiter plates to assess the mitochondrial metabolism of living cells by the MTT assay, evaluate membrane integrity with the LDH assay and assess intracellular ROS production and intracellular calcium (see below). A 6-well microtiter plate was used to assess early apoptosis or late apoptosis/necrosis with the Annexin V/PI assay.

MTT assay

PC12 and SHSY5Y cell lines were seeded in 200 µL growth medium to a density of 3×10^4 and 6×10^4 cell/mL respectively and then incubated for 24 hours. Then, the cells were treated with 10% v/v αSN pre-incubated with NLPs and incubated in the same conditions for an additional 24 hours. Medium was removed, and a freshly pre-warmed medium supplemented with 10% (v/v) MTT stock solution (5 mg/mL in PBS) was added to each well followed by 4 hours incubation. Crystals of formazan were dissolved in DMSO, and absorption at 570 nm (which reflects mitochondrial metabolic activity) was recorded on a plate reader (Expert 96, AsysHitch, Ec Austria). The control sample (no αSN, no NLPs) was set to 100%. Cell viability was calculated as the absorption at 570 nm of treated cells relative to control cells.

LDH assay

Release of the cytoplasmic enzyme LDH reflects loss of membrane integrity and by inference cell death. Briefly, after the treatment of cells with αSN pre-incubated with NLPs and further incubation for 24 hours, 100 µL of growth media was added to 1 mL of the kit substrate and absorbance at 340 nm was measured for 4 min at 37° C to follow conversion of NADH to NAD^+.

Flow cytometry

We used double staining with fluorescein isothiocyanate (FITC)-conjugated Annexin V (an apoptosis marker) and the nucleus stainer propidium iodide (PI) to measure the fraction of PC12 and SHSY5Y cells undergoing apoptosis or late apoptosis/necrosis. All cells were cultured in 6-well plates (5×10^5 cell/mL), incubated for 24 hours, after which 10% v/v αSN alone, or pre-incubated with NLP-Chol and NLP-Chol-PEG, was added and incubated for 24 hours. Cells were detached using 0.25% trypsin and 1 mM EDTA, centrifuged for 5 min at 1000 rpm, and pellets were rinsed with PBS and re-suspended in 500 µl binding buffer. FITC-conjugated Annexin V and PI were added and incubated in the dark for 15 min. Samples were loaded on a BD FACS Calibur flow cytometer (Becton Dickinson Biosciences, San Jose, CA, USA) and data analyzed using Flowing Software v.2.5.

Intracellular ROS

To evaluate ROS formation in cells, 2',7' – dichlorofluorescin diacetate (DCFH-DA) can be used as it crosses the cell membrane to react with ROS and form highly fluorescent 2′, 7′–dichlorofluorescein (DCF). PC12 and SHSY5Y cells were cultured in 96-well plates at a density of 6×10^4 and 10×10^4 cell/mL respectively and incubated for 24 hours in a CO_2 incubator, after which 10% v/v αSN alone or pre-incubated with NLP-Chol and NLP-Chol-PEG was added and incubated for 24 hours. Growth media were replaced with serum-free media and 15 µM DCFH-DA was added followed by incubation for 45 min in the dark at 37 °C. Cells were rinsed twice with PBS and the fluorescence intensity was measured at excitation and emission wavelengths of 485 nm and 530 nm respectively using a Varian Cary Eclipse fluorescence spectrophotometer (Mulgrave, Australia).

Intracellular Ca^{2+} levels

Intracellular calcium levels were determined using the Ca^{2+} chelator Fura 2-AM based on the ratio of its excitation intensity at 340 and 380 nm (emission at 510 nm). SHSY5Y cells were cultured in 96-well plates (8×10^4 cell/mL) and incubated for 24 hours. The cells were then treated with 10% v/v 7 h-aged and 24 h-aged αSN pre-incubated with or without NLP-Chol and NLP-Chol-PEG. To remove background Ca^{2+}, the culture medium from 24 hours incubated cells was replaced with PBS. Intracellular calcium levels were assessed in two ways. In the first approach, after treatment with αSN, the cells were incubated for 6 hours, Fura 2-AM from a stock of 100 μM in acetone, was added to a final concentration of 2 μM, cells were incubated for 5 min in the dark and fluorescence was measured. The second approach differed from the first in omitting the 6 h incubation step, *i.e.* Fura 2-AM was added straight after adding αSN; furthermore, fluorescence was measured over a 30 min period.

Statistical analysis

All experiments were in triplicate unless otherwise stated, and results are provided as means ± SD. One-way ANOVA algorithms were used to compute the statistical significance within the groups. Unpaired Student's *t*-test was also employed to determine the significance results between the groups, where a probability value $p < 0.05$ was considered significant.

Results

NLP-Chol and NLP-Chol-PEG delay fibrillization by extending the lag phase and modifying the end point product

Here we assess the impact of uncharged NLPs with cholesterol decorated with PEG on the kinetics of αSN fibrillization. TEM and DLS revealed our NLPs to be spherical and unilamellar

uncharged NLPs (Fig. S1) with an average size of < 100 nm. To assess the influences of the NLP-Chol and NLP-Chol-PEG on the fibrillization of αSN, we incubated 70 μM αSN with 35-1500 μM NLPs and monitored fibrillization through ThT fluorescence intensity. Both NLPs decrease end-ThT levels by up to ~50% (Fig. S2) after 24 hours of incubation.

It is worth mentioning that these concentrations are in non-crowding concentration ranges. The crowding concentration is ~ 40 mg/ml and above; it is primarily considered in the framework of the excluded volume effect [33]. Herein, we examined the concentration ranges from 35-1500 μM to test whether these non-crowding concentrations have a significant impact on fibrillization. We found that at these concentrations the inhibition of fibrillization is dose-independent. To obtain more insight into the mechanistic effects of NLPs on the fibrillization process, we followed the events in detail throughout the kinetics of fibrillization at two different concentrations of NLP-Chol and NLP-Chol-PEG (140 and 280 μM), which could be suitable concentrations for drug delivery. Both NLPs increased the half time of fibrillization from ~15 to ~25 hours (Fig. 1) and the effect was similar at 140 and 280 μM. Analysis of the kinetic data using the Finke–Watzky model confirmed that both NLPs increase $t_{1/2}$ (half-time to maximum signal) and t_N (fibrillization lag phase) (Fig. 1b and c) but had no significant impact on fibrillization growth rate (Fig. 1d). This indicates that although nucleation is impeded, the subsequent elongation rate can proceed at the same rate as for untreated αSN. There is a modest decrease in the end point ThT fluorescence (Fig. 1e) suggesting that the NLPs may slightly reduce the extent of fibrillization. AFM images indicated that after 28 hours of incubation, in the presence of NLPs, low amount of fibrils were available in the samples; however, this quantity was much more in the untreated samples with NLPs demonstrating the end point products were decreased in the treated samples (Fig. S3). This alteration might result from binding the monomers or intermediate species to NLPs (Fig 2 and Fig. S4). TEM images of samples after four hours of incubation showed a mixture of fibrils and

small spherical aggregates in the control samples, while in the samples treated with NLPs a variety of small spherical aggregates were localized around the NLPs (Fig. 2a) suggesting such aggregates have an interaction with NLPs. Further incubation led to increasing amounts of fibrils in the NLPs-treated samples but non-fibrillar aggregates persisted in the NLPs samples while they completely disappeared in the control samples (Fig. 2b and c). It seems that in the presence of NLPs, there is an increase in the number of small non-fibrillar aggregates which do not then proceed to form fibrils. This is imperative because NLPs seem more likely to interact with intermediate aggregated species rather than monomers and to stabilize them, leading to a reduction in their cytotoxicity; ultimately hindering their progress towards fibrillization.

By centrifugation, it was perceived that NLPs interact with monomers and different aggregated species of αSN which were detected by SDS-PAGE. However, a dissimilar outcome was detected at 48 hours for αSN incubated alone. This is consistent with NLPs having an interaction with monomers and small species of αSN aggregate (Fig. S4). At low speed of centrifugation (5000 rpm for 10 min), the protein interacting with NLPs was precipitated and consistently in the supernatant a lower amount of protein was detected. At high speed of centrifugation (13000 rpm for 30 min), more precipitated particles were identified in samples without NLPs. With respect to our experience and previous studies, some intermediates of αSN aggregation are SDS resistant [34], however, fibrils are characterized as SDS sensitive structures that can be partially disassembled in the presence of SDS and appear as a monomeric band in SDS-PAGE [35].

NLPs affect neither seeding nor depolymerization of the fibrils

The impact of NLPs on the ability to grow fibrils from fibrillary seeds (by inference to affect the elongation step of fibrillization) was assessed by adding sonicated mature fibrils (as shown in a TEM image, Fig. S5) to fresh monomeric αSN. The NLPs affected neither elongation kinetics

(Fig. S6a) nor did they reduce the ThT fluorescence of existing fibrils when co-incubated with or without shaking (Fig. S6b and c). Thus the NLPs do not intervene in the fibrillization process once aggregation nuclei have been formed.

Neutral NLPs bind both monomeric and oligomeric αSN, reducing reversibility of monomer-negatively charge membrane interactions probably through N-terminal interactions

Far-UV CD analysis showed that αSN goes over from random coil to β-sheet structures more slowly when treated with NLPs (Fig. 3 a-c). Moreover, the plot of the 200/220 nm of CD signal ratio revealed that results were almost consistent with our ThT outcomes (Fig. 3 d).

To identify possible interactions between αSN and the NLPs, we span down NLPs in the presence of fluorescence-labeled αSN and saw a decrease in soluble αSN, accompanied by a significant increase in the amount of αSN in the pellet (Fig. S7). Similarly, short-term incubated αSN (2-3 hours of incubation) which contains oligomeric αSN, but presumably also a significant monomer fraction) was pelleted together with NLPs (Fig. S7). Direct evidence for αSN-NLP interactions was provided by liquid-state NMR spectroscopy (Fig 4). NMR signals were broadened in the presence of NLP-Chol, particularly in the first 12 residues. Less signal broadening was observed when NLP-Chol-PEG was employed. Because the NMR experiments ran at low temperature (15 °C) and bulky PEG is less flexible at this temperature, lipid surface accessibility maybe reduced. We cannot exclude the possibility that the number and identity of residues involved in αSN binding to NLPs at higher temperatures may be different than that characterized by our current NMR data. Another point is that in many circumstances, the NLPs interact with intermediate species like oligomers that cannot easily be recognized with NMR. Nonetheless, in the TEM experiments we found that many oligomers are present in treated

samples even after a long incubation time. We concluded that the interaction also occurs between NLPs and oligomers.

Another way to probe interactions was to carry out thermal scans in the presence of anionic vesicles made using DMPG. Such vesicles bind αSN and induce α-helical structure as the temperature increases from 10 to 30-40 °C (Fig 5a); this structure melts out at higher temperatures and the whole process is essentially completely reversible. However, adding either NLP-Chol or NLP-Chol-PEG to the DMPG/αSN mix severely reduces the reversibility of this process (Fig. 5b and c), indicating that neutral phospholipids can impede the interaction of the protein with DMPG. Nevertheless, this is a competitive interaction between uncharged and negatively charged vesicles. We also detect this phenomenon with oligomeric forms. Calcein release from DOPG vesicles by αSN oligomers (prepared by gel filtration, Fig. S8a) was not affected by the presence of 10-80 μM NLP-Chol and NLP-Chol-PEG (Fig. S8b, c). Further, NLP-Chol or NLP-Chol-PEG alone had no influence on membrane permeabilization (Fig S8d and e).

Neurotoxicity of aggregated species of αSN reduced by NLPs

To assess whether treatment of αSN with NLPs during the fibrillization process had an influence on its cytotoxicity, MTT and LDH assays were carried out. NLPs alone did not show any cytotoxicity (Fig S9). MTT assay (Fig S10a and b) revealed that all concentrations (35-1500 μM) of either NLP-Chol or NLP-Chol-PEG decreased the cytotoxicity of αSN aggregates in both cell lines after 24 hours of incubation. These outcomes were confirmed by LDH assay (Fig S10c and d). Furthermore, adding 280 μM NLPs decreased cytotoxicity of different species of αSN aggregates produced during the fibrillization (Fig 6a and b). Although intermediate/non-fibrillar aggregates in the treated samples with NLPs were greater than that of control, and the control

sample had more fibrils (Fig. 2), no considerable toxicity was observed when αSN was incubated with NLPs (more intermediate aggregates available). This is a critical point as the oligomers/intermediate aggregates have been reported to be more toxic than mature fibrils. This could be due to the interaction of such intermediate aggregates with NLPs leading then most probably to change their structures or conformations which causes less cytotoxicity. This interaction can especially influence on the membrane-permeabilizing effects of oligomers or even cause generation of the non-fibrillar aggregates which cannot continue the fibrillization process. Such aggregates may be off-pathway or amorphous aggregates which have less cytotoxicity. As we observed from Fig 1d, the final products in the presence of NLPs were also decreased compared to that of control, corroborating this outcome. In a recent study supporting this idea, it was demonstrated that binding nanobodies to αSN induced a fast conformational alteration from more stable oligomers to less stable oligomers of αSN, and this consequently caused an intense decrease in oligomer cytoxicity [36].

Apoptosis is one of the primary cell death pathways in neurodegenerative diseases and hence, using flow cytometry, the cell death arising from αSN was explored (Fig 7). The rate of early apoptosis as well as late apoptosis/necrosis in the samples treated with αSN alone is rather more than those treated with αSN pre-incubated in the presence of NLPs and this quantity is more evident in the late apoptosis/necrosis stage, especially for SHSY5Y. Finally, we note that the NLPs are biocompatible in hemolysis tests (Fig. S11). In this test the amount of lysis of red blood cells is categorized with different colors occurring in the media after treatment [37].

Neurotoxic intercellular events modified when αSN pre-incubated with NLPs

Changes in ROS levels and calcium homeostasis have been implicated in neurodegeneration. While neither NLP types affected ROS and the level of free radicals *in vitro* or in cells by

themselves (Fig. S12), they reduced ROS levels in cells treated with different pre-formed αSN (70 μM) aggregates (aged for 7, 12 and 24 hours) compared to the ROS level in the control (Fig 8). By comparison, the intracellular calcium did not change significantly (Fig. S13a), even when the measurement was carried out immediately after treatment in a continuous manner (Fig. S13b and c), suggesting an alternative mechanism is involved in neurotoxic intercellular events induced by αSN.

NLPs diminish αSN aggregate neurotoxicity in SHSY5Y cells overexpressing αSN

It is interesting that the NLPs protect the cells from toxic effects of αSN even in the cells overexpressing αSN (Fig 9a). Furthermore, in order to make system more susceptible, sonicated 48-h aged incubated αSN was added to cells as seeds to trigger the fibrillization process. Here again we found that the presence of NLPs reduced the cytotoxicity of αSN (Fig 9a). ROS levels were also modified for cells treated with aggregated species of αSN in the presence of NLPs (Fig 9b).

Discussion

This work is part of our ongoing study regarding the employment of zwitterionic NLPs as suitable carriers for treating neurodegenerative diseases, especially PD. Here, we have used zwitterionic phospholipids (DPPC) to formulate NLPs incorporated and decorated with cholesterol and PEG, respectively, motivated by their similarity to the neuronal plasma membrane [11]. Both NLPs impeded fibrillization by increasing the lag phase and modestly reducing the extent of fibrillization. The key to this is likely the NLPs' interaction with monomeric and oligomeric αSN which reduces the amount of αSN available for aggregation. The interaction with αSN monomers/oligomers highlights an inhibitory role for NLPs by interfering with fibrillization.

Membranes can provide an interface that the protein might use for nucleation and drive fibril formation or be stabilized in its monomeric form, or even form the off-pathway oligomers [16]. Moreover, the effect of NLPs' charge on the interaction and fibril formation of αSN is a subject of controversy. Although the interaction of negatively charged NLP with αSN has been established [17], the feasibility of binding of αSN to zwitterionic lipid vesicles is controversial. Some studies reported that αSN does not bind to zwitterionic/uncharged lipid membrane [10,17,38,39]; however, some indicate a weak interaction [12,22,40] and other reports imply a strong interaction between them [18,41]. This interaction can even remodel neutral vesicles into tubules [12]. Here, we found an interaction between zwitterionic NLPs and αSN.

Cholesterol may have a role in the interaction between NLPs and αSN. Two discrete cholesterol-binding domains in αSN have been recognized, residues 67–78 which have high affinity to bind cholesterol, and residues 34–45 which have lower affinity. In addition, αSN has been demonstrated to bind to the isooctyl chain of cholesterol in membranes [42,43]. Cholesterol also increases the order of the membrane while maintaining lipid fluidity [44]. Cholesterol has been shown to mediate the interaction between oligomers of αSN and zwitterionic membranes [44].

Interestingly, NLPs reduce the reversibility of thermal melting of membranes of anionic vesicles, suggesting that once thermally denatured, αSN remains more strongly bound to NLPs and is therefore not able to rebind to vesicles. The interaction appears to involve the very N-terminal region of αSN which is also strongly implicated in membrane binding [17], suggesting a competition between anionic vesicles and NLPs for binding to this region. However, the interaction is sufficiently weak that NLPs do not prevent monomeric αSN from binding to preexisting fibrils to elongate them. Thus only the initial stage of fibrillization is affected,

probably because it is more sensitive to even a slight decrease in the amount of free and unimpeded αSN in the formation of the fibrillization nucleus.

Conclusion

Taken together, we conclude that at the first stage of fibrillization process, some monomers and oligomers interact with NLPs at the expense of fibrillization. We summarize our insights in Fig 10: I) Interactions between the NLPs and αSN, likely correlated to the presence of cholesterol/PEG, impede the early stages of fibrillization. Given the absence of overall charge in the DPPC vesicles, hydrophobic interactions are likely the dominant factors in the binding of αSN to zwitterionic lipid vesicles [22]. II) As the oligomers are more hydrophobic [45], they are more likely to interact through their hydrophobic regions with liposomal membranes. III) As a consequence, NLPs reduce the amount of free oligomer and monomeric αSN, which not only impedes fibrillization but also reduces neurotoxicity and ROS levels. It has been assumed that in the systems of fibrillization, the progression of the fibril formation competes with substitute reactions including the formation of stable off-pathway oligomers or amorphous aggregation [46]. Considering that different species of aggregates are formed in the development of amyloid formation of αSN [47,48], it can be concluded that NLPs may affect one or more of these stages, by postponing the direct reaction and/or stimulating the reverse reaction; subsequently affecting the cytotoxic effects of the species produced. These findings could open a new avenue in the use of NLPs to combat neurodegenerative diseases, and for use as a vehicle for drug delivery given their ability to take up and transport both hydrophobic and hydrophilic small molecules alongside their intrinsic ability to delay the aggregation process leading to a reduction of both neurotoxicity and ROS levels. In this regard, we have recently illustrated the capability of this type of NLP for transferring both hydrophobic and hydrophilic small molecules into cells [37]. These results can help us to establish the therapeutic potential of such NLPs.

Acknowledgment

This study was supported by National Institute of Genetic Engineering and Biotechnology, Tehran, Iran (Grant nr. 940701-I-523). D.E.O. is supported by the Danish Research Council Medical Sciences (Grant nr. 4183-00225) and the Lundbeck Foundation (Grant nr. R180-2014-3545). MZ was supported by the Cluster of Excellence and DFG Research Center Nanoscale Microscopy and Molecular Physiology of the Brain. Karin Giller is acknowledged for preparation of NMR samples. Miss Seyedeh Flour Mazhar is also acknowledged for helping us to perform hemolysis tests.

References

1 M. G. Spillantini, M. L. Schmidt, V. M.-Y. Lee, J. Q. Trojanowski, R. Jakes and M. Goedert, *Nature*, 1997, **388**, 839–840.

2 A.-L. Mahul-Mellier, F. Vercruysse, B. Maco, N. Ait-Bouziad, M. De Roo, D. Muller and H. A. Lashuel, *Cell Death Differ.*, 2015, **22**, 2107–2122.

3 Y. Liu, J. A. Carver, A. N. Calabrese and T. L. Pukala, *Biochim. Biophys. Acta - Proteins Proteomics*, 2014, **1844**, 1481–1485.

4 D. Morshedi, F. Aliakbari, A. Tayaranian-Marvian, A. Fassihi, F. Pan-Montojo and H. Pérez-Sánchez, *J. Food Sci.*, 2015, **80**, H2336–H2345.

5 N. Taebnia, D. Morshedi, S. Yaghmaei, F. Aliakbari, F. Rahimi and A. Arpanaei, *Langmuir*, 2016, **32**, 13394–13402.

6 C. A. Braga, C. Follmer, F. L. Palhano, E. Khattar, M. S. Freitas, L. Romão, S. Di Giovanni, H. A. Lashuel, J. L. Silva and D. Foguel, *J. Mol. Biol.*, 2011, **405**, 254–273.

7 W. I. Rosenblum, *Neurobiol. Aging*, 2014, **35**, 969–974.

8 K. C. Luk, V. Kehm, J. Carroll, B. Zhang, P. O'Brien, J. Q. Trojanowski and V. M.-Y. Lee, *Science (80-.).*, 2012, **338**, 949–953.

9 J. F. Reyes, T. T. Olsson, J. T. Lamberts, M. J. Devine, T. Kunath and P. Brundin, *Neurobiol. Dis.*, 2015, **77**, 266–275.

10 W. S. Davidson, A. Jonas, D. F. Clayton and J. M. George, *J. Biol. Chem.*, 1998, **273**, 9443–9.

11 L. Lim and M. R. Wenk, in *Handbook of Neurochemistry and Molecular Neurobiology*, Springer US, Boston, MA, 2009, pp. 223–238.

12 Z. Jiang, M. de Messieres and J. C. Lee, *J. Am. Chem. Soc.*, 2013, **135**, 15970–15973.

13 P. H. Jensen, M. S. Nielsen, R. Jakes, C. G. Dotti and M. Goedert, *J. Biol. Chem.*, 1998,

273, 26292–4.

14 L. Kjaer, L. Giehm, T. Heimburg and D. Otzen, *Biophys. J.*, 2009, **96**, 2857–2870.

15 C. Galvagnion, *J. Parkinsons. Dis.*, 2017, **7**, 433–450.

16 C. Galvagnion, J. W. P. Brown, M. M. Ouberai, P. Flagmeier, M. Vendruscolo, A. K. Buell, E. Sparr and C. M. Dobson, *Proc. Natl. Acad. Sci.*, 2016, **113**, 7065–7070.

17 M. Zhu and A. L. Fink, *J. Biol. Chem.*, 2003, **278**, 16873–16877.

18 V. Narayanan and S. Scarlata, *Biochemistry*, 2001, **40**, 9927–34.

19 H.-J. Lee, C. Choi and S.-J. Lee, *J. Biol. Chem.*, 2002, **277**, 671–8.

20 S. Ghio, F. Kamp, R. Cauchi, A. Giese and N. Vassallo, *Prog. Lipid Res.*, 2016, **61**, 73–82.

21 C. Galvagnion, A. K. Buell, G. Meisl, T. C. T. Michaels, M. Vendruscolo, T. P. J. Knowles and C. M. Dobson, *Nat. Chem. Biol.*, 2015, **11**, 229–234.

22 E. R. Middleton and E. Rhoades, *Biophys. J.*, 2010, **99**, 2279–2288.

23 M. Gregori, M. Taylor, E. Salvati, F. Re, S. Mancini, C. Balducci, G. Forloni, V. Zambelli, S. Sesana, M. Michael, C. Michail, C. Tinker-Mill, O. Kolosov, M. Sherer, S. Harris, N. J. Fullwood, M. Masserini and D. Allsop, *Nanomedicine Nanotechnology, Biol. Med.*, 2017, **13**, 723–732.

24 A. Akbarzadeh, R. Rezaei-Sadabady, S. Davaran, S. W. Joo, N. Zarghami, Y. Hanifehpour, M. Samiei, M. Kouhi and K. Nejati-Koshki, *Nanoscale Res. Lett.*, 2013, **8**, 102.

25 G. Bozzuto and A. Molinari, *Int. J. Nanomedicine*, 2015, **10**, 975.

26 P. I. Campbell, *Cytobios*, 1983, **37**, 21–6.

27 K. B. Knudsen, H. Northeved, P. Kumar EK, A. Permin, T. Gjetting, T. L. Andresen, S. Larsen, K. M. Wegener, J. Lykkesfeldt, K. Jantzen, S. Loft, P. Møller and M. Roursgaard, *Nanomedicine Nanotechnology, Biol. Med.*, 2015, **11**, 467–477.

28 G. Smistad, J. Jacobsen and S. A. Sande, *Int. J. Pharm.*, 2007, **330**, 14–22.

29 F. Aliakbari, A. A. Shabani, H. Bardania, H. A. Eslampanah Seyedi, H. Mohammad-Beigi, A. Tayaranian Marvian, M. Nassoti, A. A. Vafaei, S. A. Shojaosadati, A. A. Saboury, G. Christiansen and D. Morshedi, *Sharif Univ. Technol.*, , DOI:10.24200/SCI.2017.4419.

30 J.-P. Liu, Y. Tang, S. Zhou, B. H. Toh, C. McLean and H. Li, *Mol. Cell. Neurosci.*, 2010, **43**, 33–42.

31 A. M. Morris, M. A. Watzky, A. Jeffrey N. Agar and R. G. Finke, *Biochemistry*, 2008, **47**, 2413–2427.

32 D. Morshedi and M. Nasouti, *Parkinsons. Dis.*, 2016, **2016**, 1–10.

33 V. N. Uversky, E. M. Cooper, K. S. Bower, J. Li and A. L. Fink, *FEBS Lett.*, 2002, **515**, 99–103.

34 L. Pieri, K. Madiona and R. Melki, *Sci. Rep.*, 2016, **6**, 24526.

35 J. E. Yang, K. Y. Rhoo, S. Lee, J. T. Lee, J. H. Park, G. Bhak and S. R. Paik, *Sci. Rep.*, 2017, **7**, 17945.

36 M. Iljina, L. Hong, M. H. Horrocks, M. H. Ludtmann, M. L. Choi, C. D. Hughes, F. S. Ruggeri, T. Guilliams, A. K. Buell, J.-E. Lee, S. Gandhi, S. F. Lee, C. E. Bryant, M. Vendruscolo, T. P. J. Knowles, C. M. Dobson, E. De Genst and D. Klenerman, *BMC Biol.*, 2017, **15**, 57.

37 F. Aliakbari, A. A. Shabani, H. Bardania, H. Mohammad-Beigi, A. Tayaranian Marvian, F. Dehghani Esmatabad, A. A. Vafaei, S. A. Shojaosadati, A. A. Saboury, G. Christiansen, D. E. Otzen and D. Morshedi, *Colloids Surfaces B Biointerfaces*, 2018, **161**, 578–587.

38 E. Jo, J. McLaurin, C. M. Yip, P. St George-Hyslop and P. E. Fraser, *J. Biol. Chem.*, 2000, **275**, 34328–34.

39 M. Ramakrishnan, P. H. Jensen and D. Marsh, *Biochemistry*, 2003, **42**, 12919–12926.

40 E. Rhoades, T. F. Ramlall, W. W. Webb and D. Eliezer, *Biophys. J.*, 2006, **90**, 4692–4700.

41 B. Nuscher, F. Kamp, T. Mehnert, S. Odoy, C. Haass, P. J. Kahle and K. Beyer, *J. Biol. Chem.*, 2004, **279**, 21966–21975.

42 J. Fantini and F. J. Barrantes, *Front. Physiol.*, 2013, **4**, 31.

43 J. Fantini, D. Carlus and N. Yahi, *Biochim. Biophys. Acta - Biomembr.*, 2011, **1808**, 2343–2351.

44 A. van Maarschalkerweerd, V. Vetri and B. Vestergaard, *FEBS Lett.*, 2015, **589**, 2661–2667.

45 U. Sengupta, M. J. Guerrero-Muñoz, D. L. Castillo-Carranza, C. A. Lasagna-Reeves, J. E. Gerson, A. A. Paulucci-Holthauzen, S. Krishnamurthy, M. Farhed, G. R. Jackson and R. Kayed, *Biol. Psychiatry*, 2015, **78**, 672–683.

46 V. N. Uversky and A. L. Fink, *Biochim. Biophys. Acta - Proteins Proteomics*, 2004, **1698**, 131–153.

47 D. Morshedi, N. Rezaei-Ghaleh, A. Ebrahim-Habibi, S. Ahmadian and M. Nemat-Gorgani, *FEBS J.*, 2007, **274**, 6415–6425.

48 M. R. Cookson, *Mol. Neurodegener.*, 2009, **4**, 9.

Figure. 1.

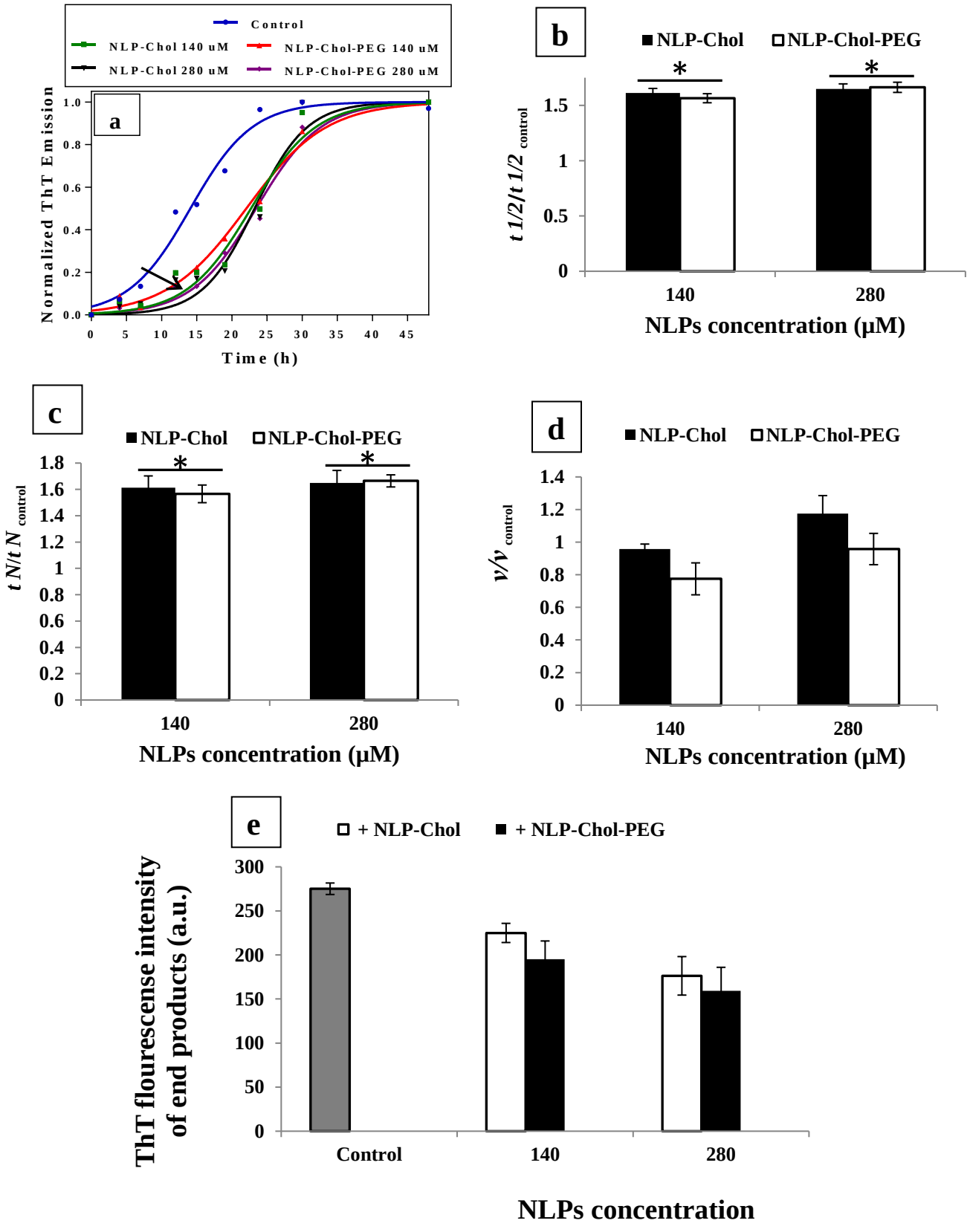
Control
NLP-Chol 140 uM
NLP-Chol-PEG 140 uM
NLP-Chol 280 uM
NLP-Chol-PEG 280 uM
a
Normalized ThT Emission
Time (h)
b
NLP-Chol
NLP-Chol-PEG
t 1/2/t 1/2 control
NLPs concentration (µM)
c
t N/t N control
d
v/v control
e
+ NLP-Chol
+ NLP-Chol-PEG
ThT flourescense intensity of end products (a.u.)
Control
NLPs concentration

Figure. 1. The effect of the NLP-Chol and NLP-Chol-PEG on the kinetics of αSN fibrillization. (a) The ThT data of the aggregation kinetic of αSN were normalized and the Finke–Watzky model was fitted to the normalized data. Arrow indicates extension in lag phase. The excitation and emission for ThT were set at 440 and 480 nm respectively. (b-d) Kinetic parameters for αSN fibril formation at 140 and 280 μM NLP-Chol and NLP-Chol-PEG relative to those values in the absence of the NLPs. (b) relative half time ($t_{1/2}/t_{1/2control}$), and (c) relative lag time ($tN/tN_{control}$), the half and lag time of αSN incubated in the presence of NLPs was considerably different from that of the control condition of αSN incubated alone (* indicates $p \leq 0.05$). (d) relative growth rate ($v/v_{control}$), the growth rate of the fibrillization was not considerably altered in the presence or absence of NLP. (e) final amount of αSN aggregation in the presence or absence of NLPs.

Figure. 2.

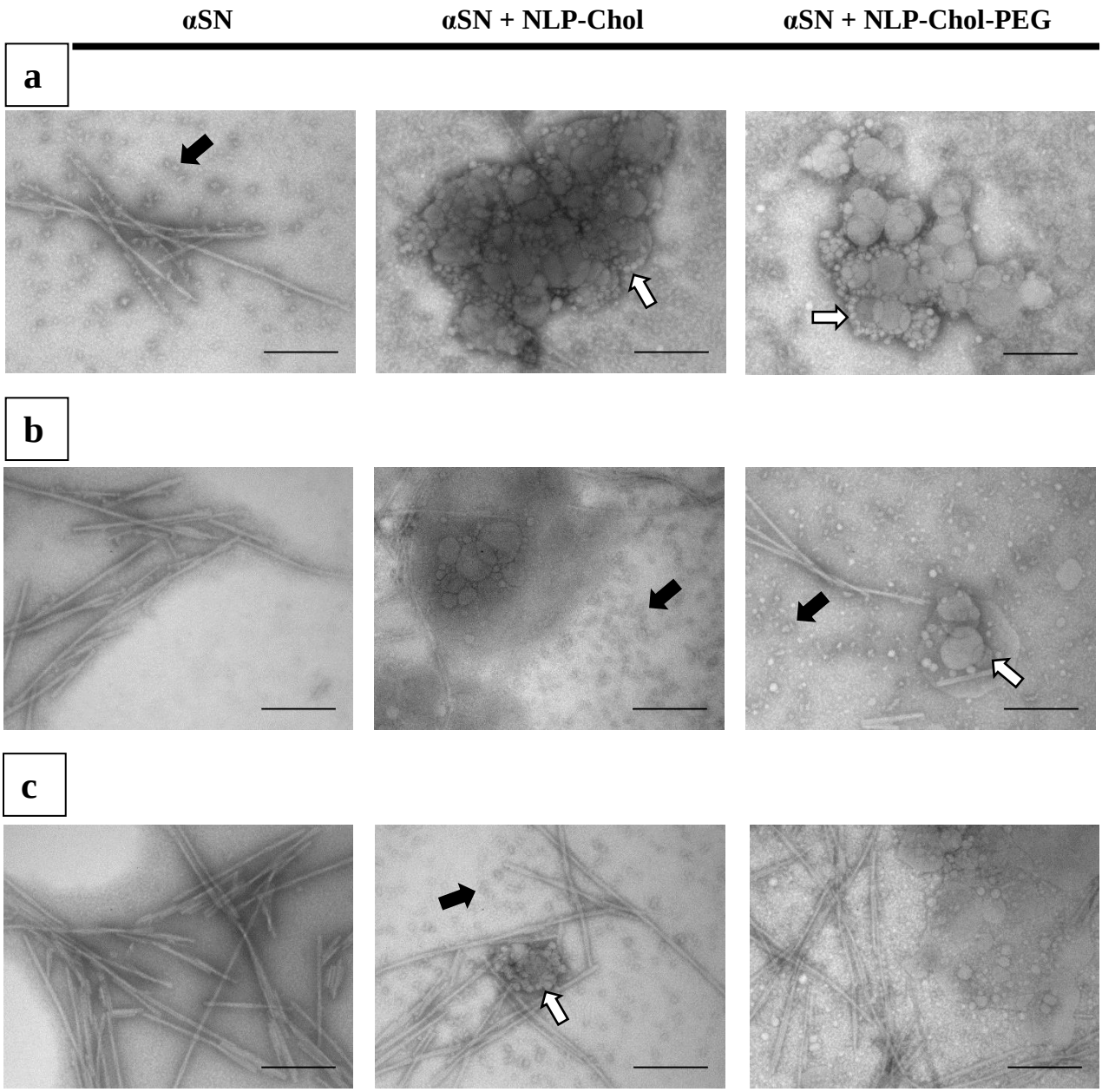

Figure. 2. TEM images over time for αSN incubated in the presence or absence of NLP-Chol and NLP-Chol-PEG. Oligomers cluster around the surface of NLPs. The images represent αSN incubated without (left) or with NLP-Chol (middle) and NLP-Chol-PEG (right) after 4 h (a), 12 h (b), 24 h (c). The white arrows indicate oligomers interacting with NLPs and the black arrows indicate free oligomers. Scale bar, 200 nm. At the early stage of fibrillization, after 4 hours of incubation, (a) the fibrils and oligomers are formed in the control sample while in the samples treated with either NLP-Chol or NLP-Chol-PEG the vesicles are covered with oligomers even after 12 hours of incubation (b). In the control sample after 12 hours incubation, thin fibrils and some oligomers was detected whereas in the treated samples with NLPs aggregated vesicles, oligomers and fibrils (in low density) are observed. Despite the increase in fibrils in all samples (c), there are more fibrils in the control sample.

Figure. 3.

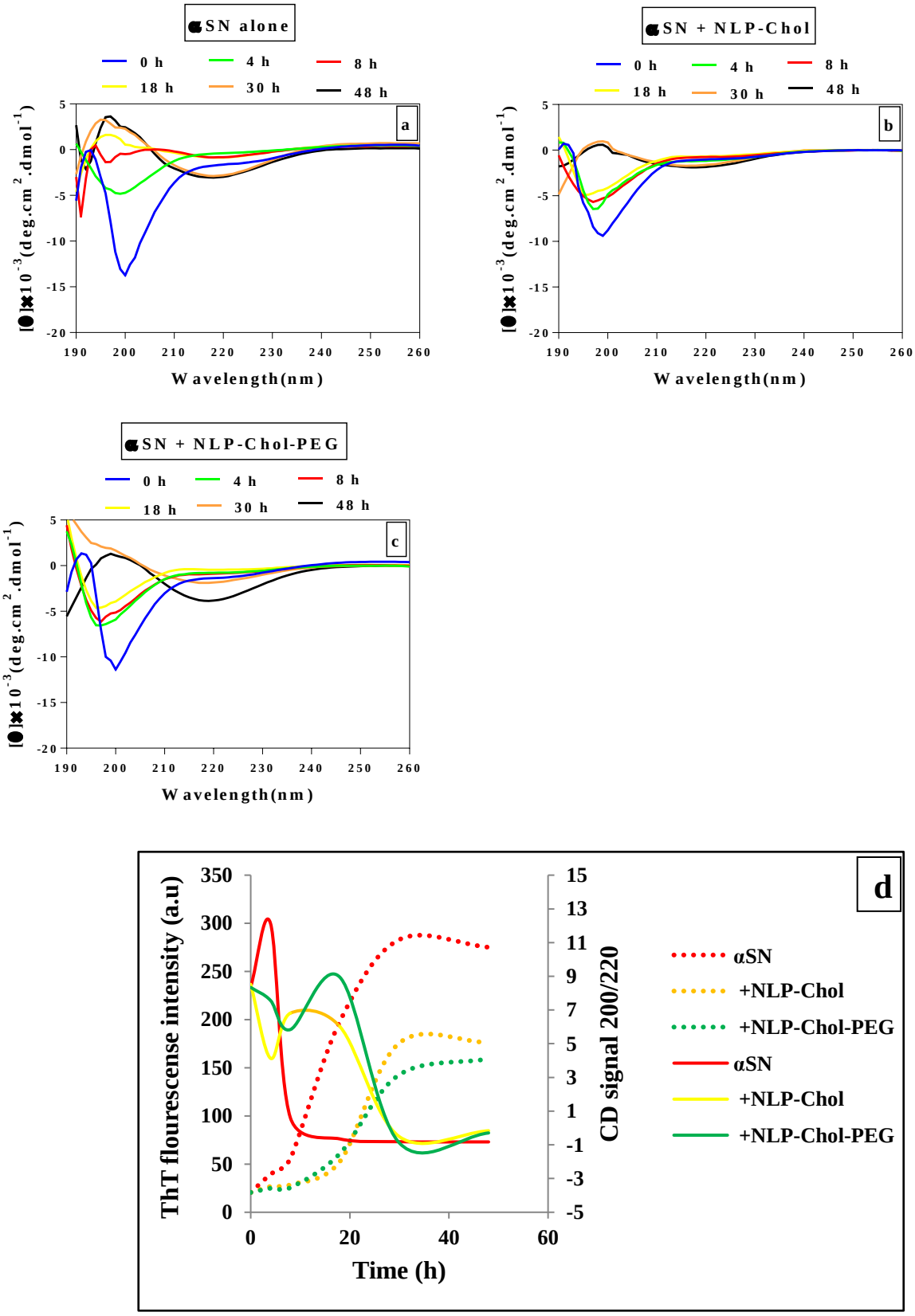
αSN alone
0 h
4 h
8 h
18 h
30 h
48 h
a
[θ]×10⁻³(deg.cm².dmol⁻¹)
Wavelength(nm)
αSN + NLP-Chol
b
αSN + NLP-Chol-PEG
c
ThT flourescense intensity (a.u)
CD signal 200/220
Time (h)
d
αSN
+NLP-Chol
+NLP-Chol-PEG

Figure. 3. Far-UV CD spectra of the αSN (70 μM) incubated in the presence or absence of 280 μM NLP-Chol or NLP-Chol-PEG. αSN incubated with NLPs displayed retained its structure up to more than 18 hours relative to αSN alone. The spectra represent αSN incubation in the absence (a) or presence of NLP-Chol (b) and NLP-Chol-PEG (c). The ratio 200/220 nm of CD signal versus time for graphs a-c are shown in direct comparison with the ThT results (d). The solid lines represent CD signal and dashed lines indicate ThT. The samples were diluted 10 times before running CD.

Figure. 4.

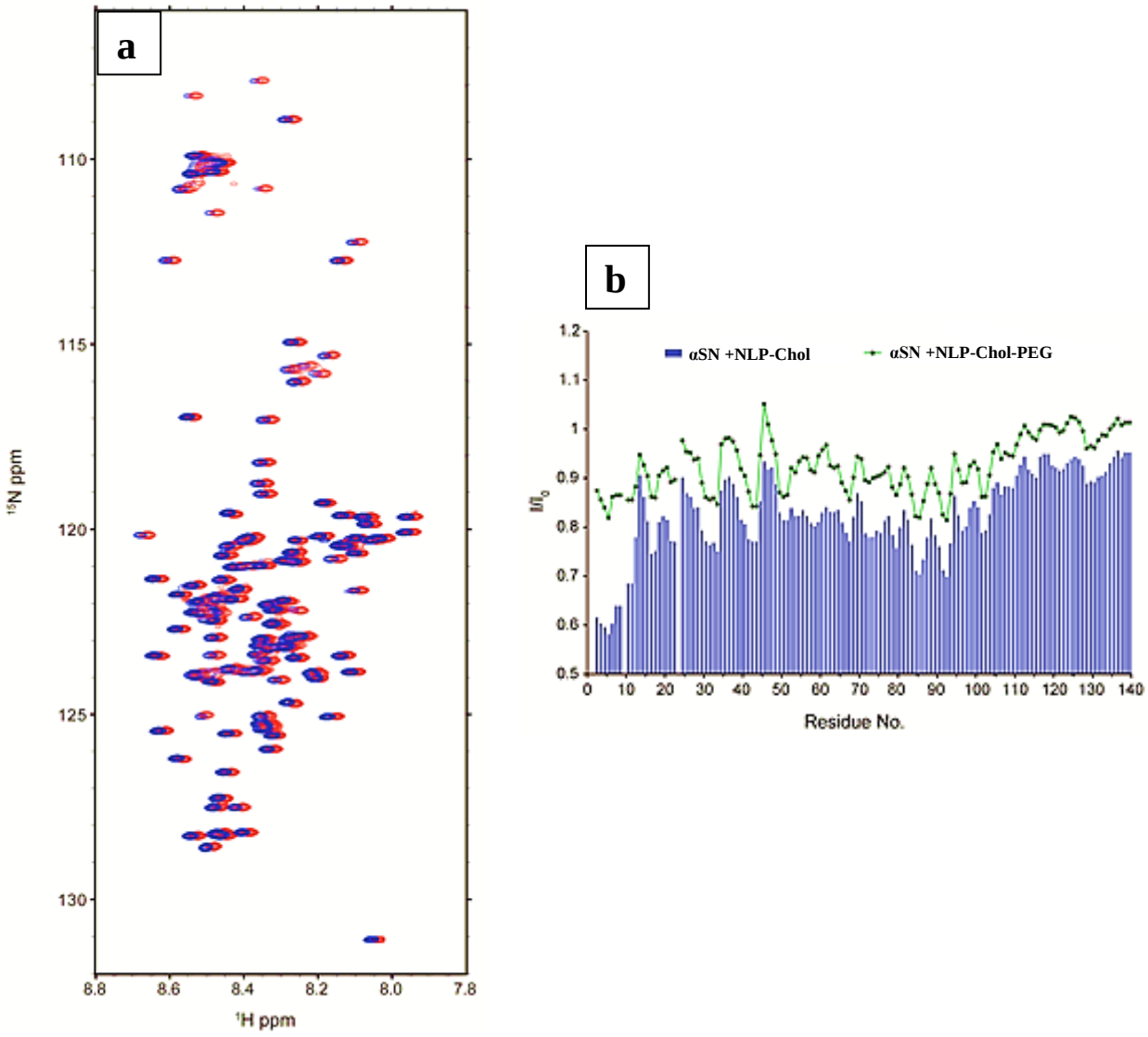

Figure. 4. Preferential interaction of the N-terminal region of αSN with NLPs. (a) Overlay of 2D ^{1}H,^{15}N HSQC spectra of αSN in the absence (red) or presence of NLP-Chol (blue). No significant chemical shift perturbation was observed. To make both datasets visible, the blue spectrum has been displaced by 0.02 ppm in the ^{1}H dimension. (b) HSQC intensity perturbation profile after addition of lipid vesicles to αSN. NMR signals originating from N-terminal residues were broadened after interaction with NLP-Chol (blue bars). Less signal broadening was observed when NLP-Chol-PEG was used (green points).

Figure. 5.

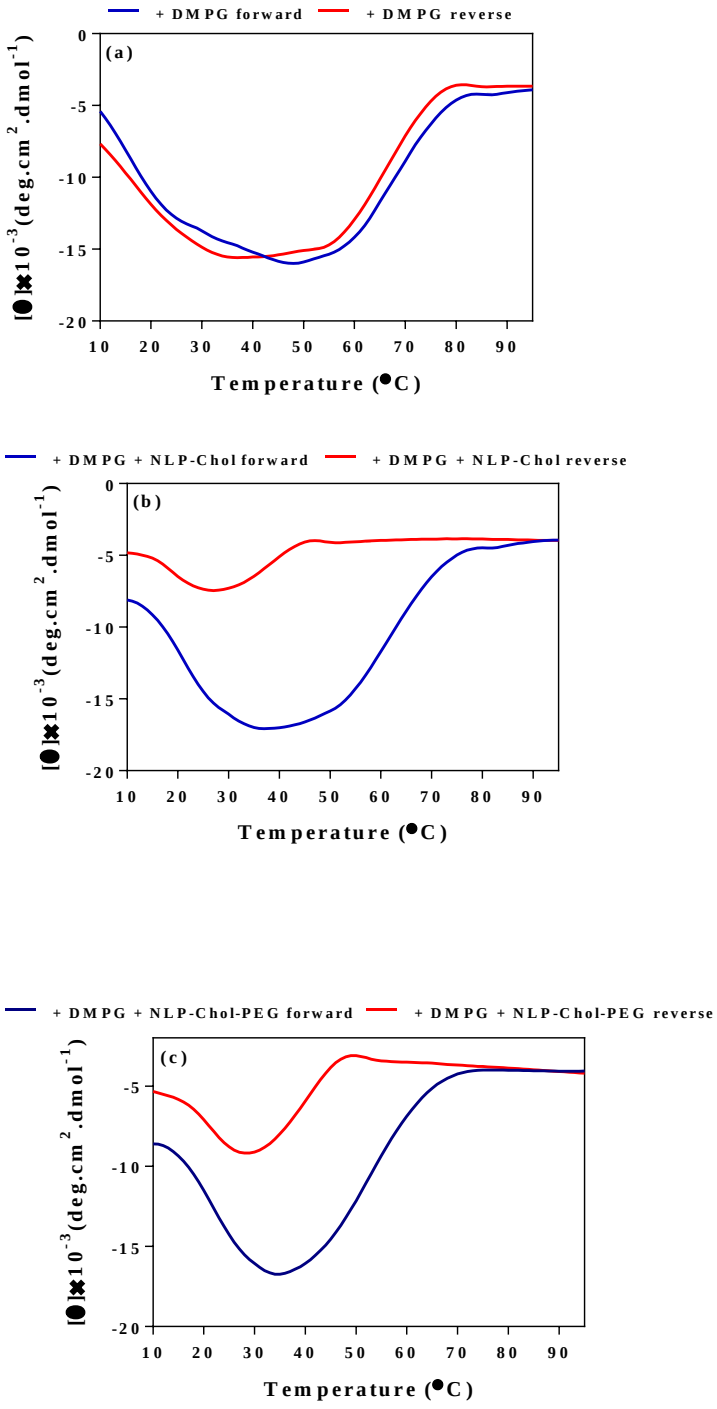

Figure. 5. Far-UV CD thermal scans (222 nm) of 7 μM αSN in the presence of 0.2 mg/ml of either DMPG (a), DMPG + NLP-Chol (100 μg/mL) (b) and DMPG + NLP-Chol-PEG (100 μg/mL) (c).

Figure. 6.

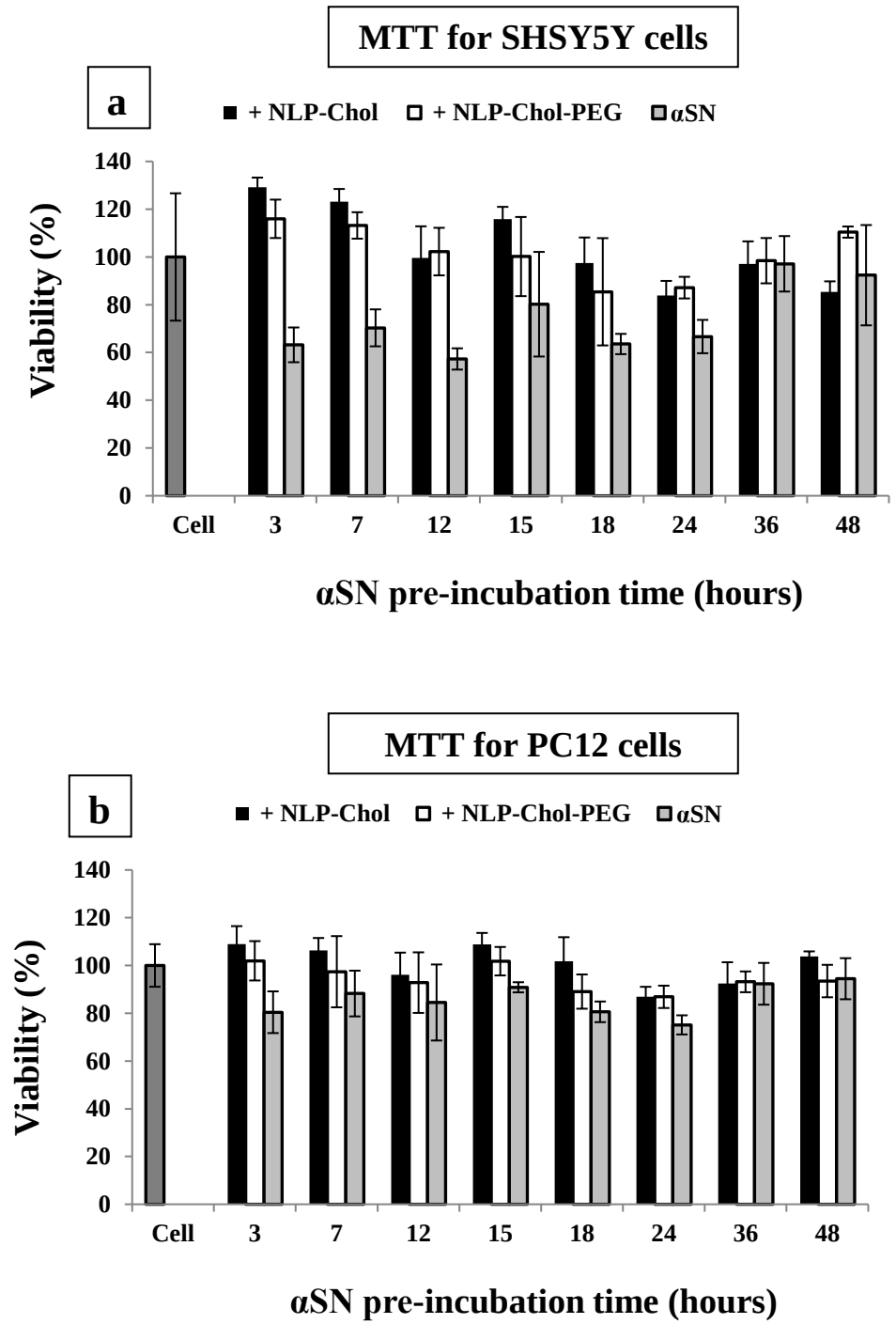

Figure. 6. Neurotoxicity of αSN (70 μM) pre-incubated 3-48 hours in the presence or absence of NLP-Chol and NLP-Chol-PEG (280 μM) using MTT after 24 hours of treatment for SHSY5Y (a) and PC12 (b) cells.

Figure. 7.

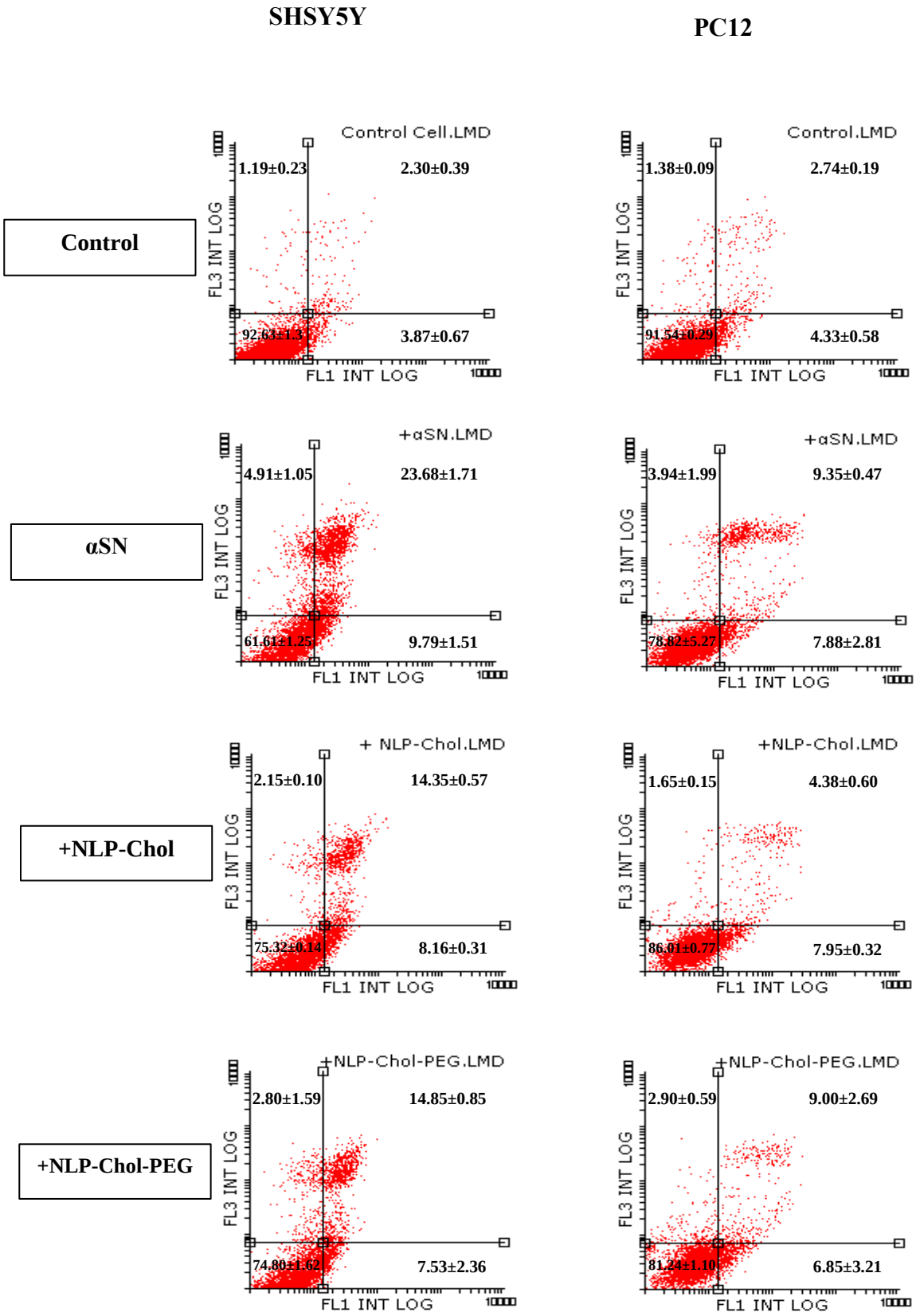
SHSY5Y
PC12
Control
αSN
+NLP-Chol
+NLP-Chol-PEG
Control Cell.LMD
Control.LMD
+αSN.LMD
+ NLP-Chol.LMD
+NLP-Chol.LMD
+NLP-Chol-PEG.LMD
FL3 INT LOG
FL1 INT LOG
1.19±0.23
2.30±0.39
92.63±1.3
3.87±0.67
1.38±0.09
2.74±0.19
91.54±0.29
4.33±0.58
4.91±1.05
23.68±1.71
61.61±1.25
9.79±1.51
3.94±1.99
9.35±0.47
78.82±5.27
7.88±2.81
2.15±0.10
14.35±0.57
75.32±0.14
8.16±0.31
1.65±0.15
4.38±0.60
86.01±0.77
7.95±0.32
2.80±1.59
14.85±0.85
74.80±1.62
7.53±2.36
2.90±0.59
9.00±2.69
81.24±1.10
6.85±3.21

Figure. 7. The amount of the early apoptosis and late apoptosis/necrosis of SHSY5Y and PC12 cells treated with αSN (70 μM) pre-incubated alone or with NLP-Chol and NLP-Chol-PEG (280 μM). αSN in the absence or presence of NLPs were put on the fibrillization process and after 24 hours samples were taken. The cells were then treated with 24 h-aged aggregated species of αSN and the amount of apoptotic/necrotic cells were assessed using flow cytometry. The percentage of apoptotic and late apoptotic/necrotic cells was measured using Flowing software 2.5.0. The flow cytometry experiments were carried out in duplicate and one diagram was shown as sample and the percentage of cell count in each quadrant was revealed as mean ± SD. In these diagrams the lower left is indicated as live cells, lower right as early apoptotic cells, upper left as necrotic cells and upper right as early apoptotic/necrotic cells.

Figure. 8.

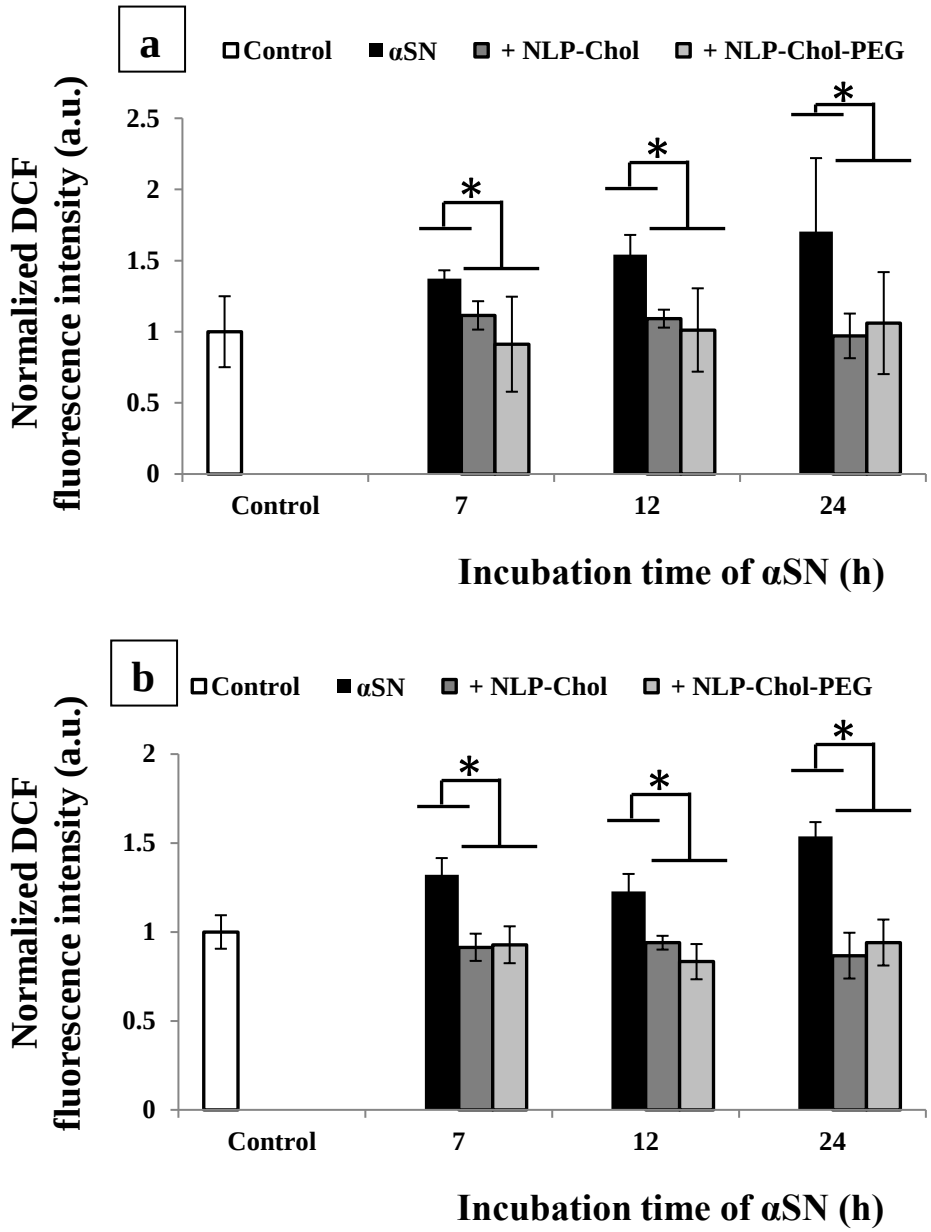

Figure. 8. The levels of intracellular ROS in SHSY5Y cells (a) and PC12 cells (b) treated with different pre-formed aggregates species of αSN (70 μM) in the absence or presence of 280 μM NLP-Chol or NLP-Chol-PEG (* indicates $p \leq 0.05$).

Figure. 9.

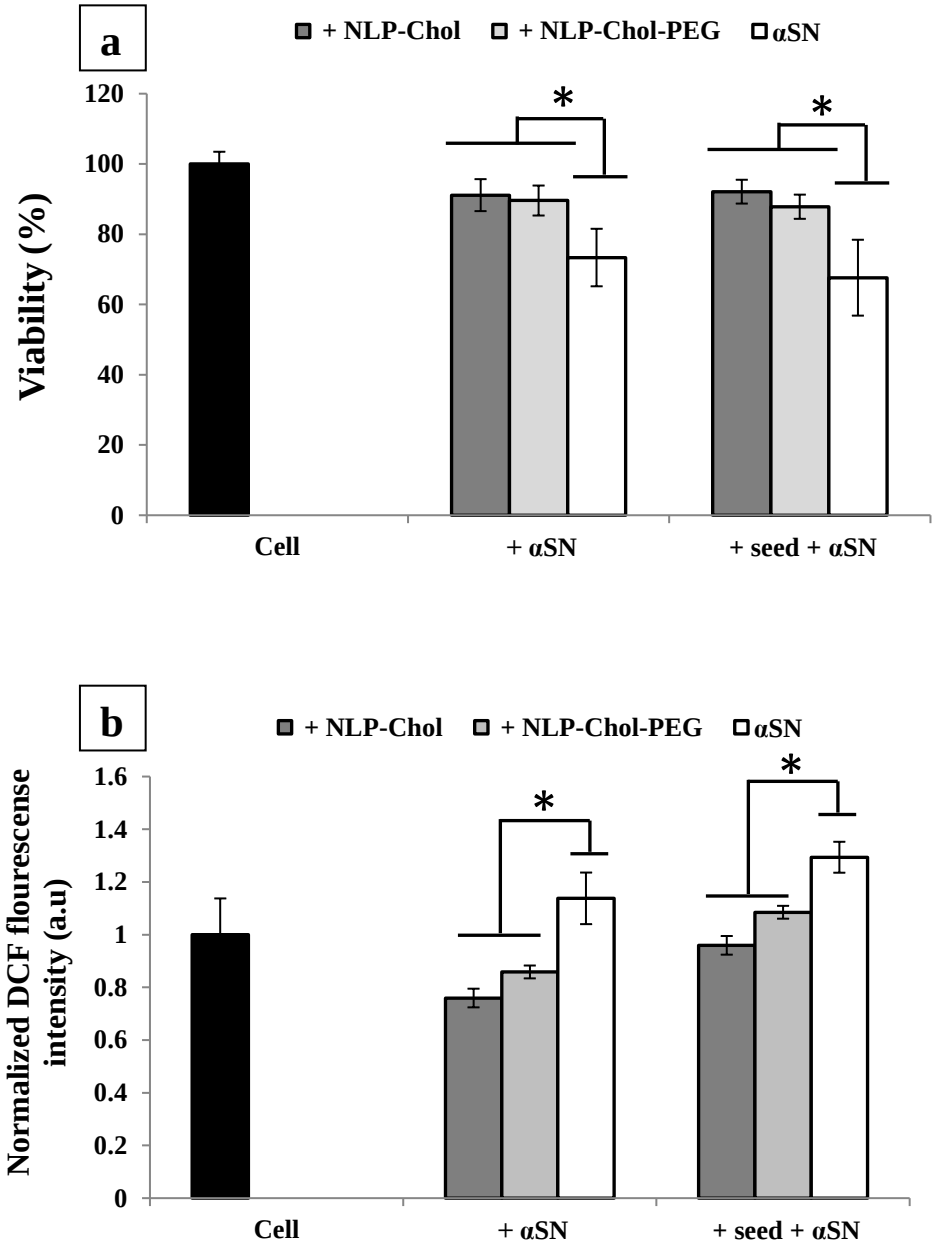

Figure. 9. Neurotoxicity of 7 h-aged aggregated species of αSN (70 μM) in the presence or absence of NLP-Chol and NLP-Chol-PEG (280 μM) on SHSY5Y cells overexpressing αSN. The cell viability and the level of intracellular ROS were evaluated using MTT (a) and DCFH-DA assay (b). Seed was the sonicated 48 h-aged αSN that was added (10% (v/v)) to cells for 2 hours before treating the cells with the above materials. Statistically significant differences between the treated samples and the control are indicated as * ($p \leq 0.05$).

Figure. 10.

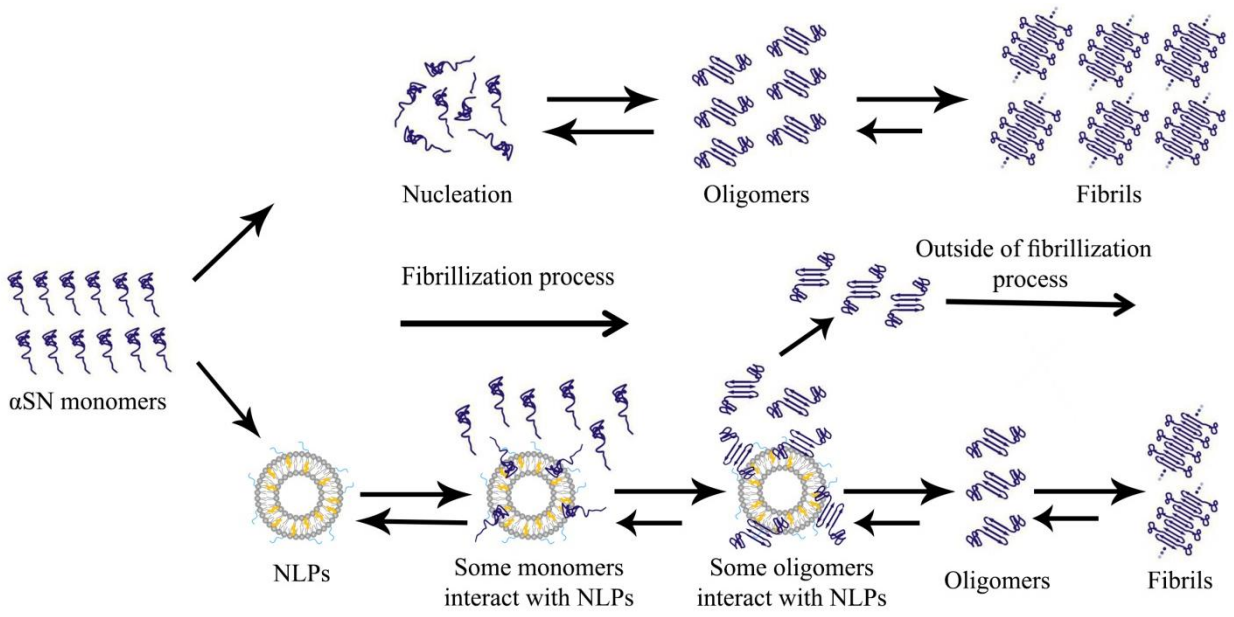

Figure. 10. Proposed mechanism for the interference of NLPs in the αSN fibrillization process leading to a reduction in fibril formation and alteration of the end product. Several reactions in this system may occur including: 1) the interaction between monomers and NLPs that different data showed to be rather weak, and so this is dynamic and reversible reaction; 2) the interaction between oligomers and NLPs that has more significant consequences. Although this reaction is also reversible, the forward reaction seems to dominate according to the results and the presence of NLPs induces the specific structures in these intermediates which cannot continue along the fibrillization pathway but form amorphous aggregates, leading to reduced cytotoxicity.